INTERNATIONAL JOURNAL OF
NUMERICAL ANALYSIS AND MODELING, *SERIES B*
Volume 5, Number 4, Pages 317–338

IMPROVING NUMERICAL ACCURACY IN A REGULARIZED BAROTROPIC VORTICITY MODEL OF GEOPHYSICAL FLOW

IGOR OLIVEIRA MONTEIRO AND CAROLINA CARDOSO MANICA

Abstract. We study the BV-α-Deconvolution model. It is a family of regularizations of the Barotropic Vorticity (BV) model that generalize the BV-α model and improve its accuracy. A both unconditionally stable and optimally convergent scheme for the BV-α-Deconvolution model is proposed and we show that it is $O(\alpha^{2N+2})$, where N is the deconvolution order, whereas the BV-α model is at most second order accurate. We perform numerical simulations to confirm the predicted convergence rates and test the model in the traditional double gyre wind experiment. For the latter test, we show that the BV-α-Deconvolution model can retrieve the expected high resolution pattern being more accurate for larger values of deconvolution order.

Key words. Barotropic vorticity model, regularizations, turbulence, geophysical flow.

1. Introduction

Accurate simulations of geophysical flows are critically important in understanding climate change and ocean and weather forecast. Furthermore, they can assist in prediction of biological and pollutant transport, oil exploration, and many other applications. One of the simplest nonlinear models to simulate a geophysical flow is the Barotropic Vorticity (BV) model, which, in dimensionless, form is given by [8, 22]

$$Ro\,\frac{\partial \omega}{\partial t} + Ro\,J(\psi,\omega) - \frac{\partial \psi}{\partial x} - \left(\frac{\delta_M}{L}\right)^3 \Delta\omega = \mathcal{F}, \tag{1a}$$

$$\Delta\psi = -\omega, \tag{1b}$$

where ω is the vorticity, ψ is the streamfunction, $J(\psi,\omega) = \frac{\partial \psi}{\partial x}\frac{\partial \omega}{\partial y} - \frac{\partial \psi}{\partial y}\frac{\partial \omega}{\partial x}$ is the Jacobian, Ro is the Rossby number, δ_M is the Munk scale, L is the length scale and $\mathcal{F}$ is the forcing term. The BV model is widely used to study the midlatitude, wind-driven ocean circulation, and it recently has been used in studies involving data assimilation [27, 4, 9], climate [19, 14, 5] and oceanic and atmosphere processes [3, 25, 20].

Despite its simplicity, the BV model is very sensitive to the mesh resolution [6, 16, 8, 22], making full representation of the solution computationally expensive. This becomes critical when long time integration is necessary, as in climate modeling. Traditionally, simulations are done on coarse meshes and (essentially) dissipative techniques such as eddy viscosity parametrizations have been used to model the under-resolved scales of the flow. However, according to [8], increasing artificial viscosity tends to reduce variability, and nonlinear structures can be destroyed by excess of dissipation [6, 8]. Thus some methods such as Approximate Deconvolution Modeling [22, 21], Barotropic Vorticity-α (BV-α) [17, 16, 8] and

Received by the editors July 18, 2014 and, in revised form, September 18, 2014.

2000 *Mathematics Subject Classification.* 65M12,65M60,76D99,76U99.

Igor O. Monteiro is partially supported by PRH-PB16. Carolina C. Manica is partially supported by CNPQ, 480525/2011-0.

Barotropic Vorticity-Bardina [10] have been developed with success to improve accuracy and reduce the degrees of freedom in computational simulations. The BV-α model is a regularization of the BV model proposed in [8] that allows a significant reduction of degrees of freedom in simulations. In BV-α, the nonlinearity is altered so that the flow at length scales that are smaller than the alpha length scale are nonlinearly removed by motions at the larger scales. Thus there is seemingly no need to introduce additional dissipative terms or increase the viscosity coefficient, which is often done in the BV equations. The BV-α model is given by

$$Ro\,\tfrac{\partial \omega}{\partial t} + Ro\,J(\psi,\omega) - \tfrac{\partial \psi}{\partial x} - \left(\tfrac{\delta_M}{L}\right)^3 \Delta\omega = \mathcal{F}, \tag{2a}$$

$$\Delta\psi = -\overline{\omega}, \tag{2b}$$

$$-\alpha^2\Delta\overline{\omega} + \overline{\omega} = \omega, \tag{2c}$$

where $\overline{\omega}$ is the filtered vorticity and α is the filter length scale. A more complete description of BV-α is presented in [8].

Despite being physically accurate, the BV-α model naturally has a consistency error from the BV model. It is clear from (2) that one cannot expect accuracy better than $O(\alpha^2)$. Since frequently $\alpha = O(h)$, the BV-α model is often only second order accurate. Following [15], we attempt to fix the consistency error in the BV-α model by increasing its accuracy through the van Cittert method of approximate deconvolution [24, 1, 23]. The method constructs a family D_N of approximate inverses to the filter F as the truncation of the nonconvergent formal power series $F^{-1} = \sum_{n=0}^{\infty}(I-F)^n$:

$$D_N = \sum_{n=0}^{N}(I-F)^n. \tag{3}$$

In [18], it is shown how to apply the deconvolution operator in the Navier-Stokes-α to achieve accuracy $O(\alpha^{2N+2})$, where N is the order of deconvolution. Thus we adopt the above mentioned approach and introduce the BV-α model with deconvolution (BV-α-Deconvolution) by

$$Ro\,\tfrac{\partial \omega}{\partial t} + Ro\,J(\psi,\omega) - \tfrac{\partial \psi}{\partial x} - \left(\tfrac{\delta_M}{L}\right)^3 \Delta\omega = \mathcal{F}, \tag{4a}$$

$$\Delta\psi = -D_N\overline{\omega}, \tag{4b}$$

$$-\alpha^2\Delta\overline{\omega} + \overline{\omega} = \omega. \tag{4c}$$

The BV-α-Deconvolution model, as we will show in the next sections, will allows a reduction of degrees of freedom in simulations but with a consistency error $O(\alpha^{2N+2})$ when compared to the BV model.

The paper is organized as follows: Section 2 introduces a finite element scheme for BV-α-Deconvolution and some necessary notation and mathematical preliminaries. Section 3 presents the stability analysis of the proposed scheme. Section 4 presents the convergence analysis. Convergence rates are estimated and the double gyre experiment is performed in Section 5. Finally, some conclusions and remarks are summarized in Section 6.

2. The finite element scheme and preliminaries

Let $\Omega \subset \mathbb{R}^2$ be a polyhedral domain and τ_h be a regular discretization of Ω. Let $H^1 = H^1(\Omega)$ be the Sobolev space $W_2^1(\Omega)$ and $X := H_0^1(\Omega)$ its subspace with zero boundary condition. Let Y_h be the continuous finite element (FE) space with kth degree polynomials on each element of the triangulation τ_h, and X_h be the subspace of Y_h with zero boundary values. Denote by $\langle \cdot, \cdot \rangle$ and $\| \cdot \|$ the inner product and norm in $L^2(\Omega)$, and $\| \cdot \|_k$ the norm in the space H^k.

For continuous in time functions we denote for $1 \leq m < \infty$,

$$\|f\|_{\infty,k} := \operatorname*{ess\,sup}_{t\in(0,T)} \|f(t,\cdot)\|_k \text{ and } \|f\|_{m,k} := \left\{ \int_0^T \|f(t,\cdot)\|_k^m dt \right\}^{\frac{1}{m}}.$$

For the discrete case we denote

$$|||f|||_{\infty,k} := \operatorname*{ess\,sup}_{0\leq n\leq M} \|f^n\|_k, \ |||f^{1/2}|||_{\infty,k} := \operatorname*{ess\,sup}_{0\leq n\leq M} \|f(t^{n+\frac{1}{2}})\|_k,$$

$$|||f|||_{m,k} := \left\{ \sum_{n=0}^{M} \|f^n\|_k^m dt \right\}^{\frac{1}{m}}, \ |||f^{1/2}|||_{m,k} := \left\{ \sum_{n=0}^{M} \|f(t^{n+\frac{1}{2}})\|_k^m dt \right\}^{\frac{1}{m}}.$$

As in [22], in this work we will consider slip boundary conditions for the velocity, which translate into the homogeneous Dirichlet condition $\omega|_{\partial\Omega} = 0$ and the impermeability condition $\psi|_{\partial\Omega} = 0$. Multiplying (1) by test functions and integrating by parts we have the following variational formulation to the BV model: find $(\omega, \psi) \in X \times X$ such that

$$\left\langle \frac{\partial \omega}{\partial t}, \lambda \right\rangle + b\left(\psi, \omega, \lambda\right\rangle - \left\langle \frac{\partial \psi}{\partial x}, \lambda \right\rangle + \left(\tfrac{\delta_M}{L}\right)^3 \langle \nabla\omega, \nabla\lambda \rangle = \langle \mathcal{F}, \lambda \rangle \ \ \forall \lambda \in H_0^1, \tag{5a}$$

$$\langle \nabla\psi, \nabla\chi \rangle = \langle \omega, \chi \rangle \ \ \forall \chi \in H_0^1, \tag{5b}$$

where $b\left(\cdot,\cdot,\cdot\right) := \langle J\left(\cdot,\cdot\right),\cdot\rangle$ represents the trilinear form.

Analogously, the variational formulation for BV-α-Deconvolution is given by: find $(\omega, \psi, \overline{\omega}) \in X \times X \times X$ such that

$$\left\langle \frac{\partial \omega}{\partial t}, \lambda \right\rangle + b\left(\psi, \omega, \lambda\right\rangle - \left\langle \frac{\partial \psi}{\partial x}, \lambda \right\rangle + \left(\tfrac{\delta_M}{L}\right)^3 \langle \nabla\omega, \nabla\lambda \rangle = \langle \mathcal{F}, \lambda \rangle \ \ \forall \lambda \in H_0^1 \tag{6a}$$

$$\langle \nabla\psi, \nabla\chi \rangle = \langle D_N\overline{\omega}, \chi \rangle \ \ \forall \chi \in H_0^1 \tag{6b}$$

$$\alpha^2 \langle \nabla\overline{\omega}, \nabla\xi \rangle + \langle \overline{\omega}, \xi \rangle = \langle \omega, \xi \rangle \ \ \forall \xi \in H_0^1 \tag{6c}$$

where, as in [8], we considered the additional homogeneous Dirichlet condition $\overline{\omega}|_{\partial\Omega} = 0$ in the filter equation.

Now we define two projection operators useful in the subsequent analysis. Given $\xi \in X$, let $P\xi \in X^h$ be the standard L^2 orthogonal projection of ξ onto X^h such that

$$\langle \xi - P\xi, \phi \rangle = 0 \ \forall \phi \in X^h, \tag{7}$$

and let $\Pi\xi \in X^h$ be the elliptic orthogonal projection of ξ onto X^h such that

$$\langle \nabla(\xi - \Pi\xi), \nabla\phi \rangle = 0 \ \forall \phi \in X^h. \tag{8}$$

Lemma 1. *Given $\xi \in H^k$ we have the following estimates* [26]

$$\text{i) } \|\xi - P\xi\| \leq Ch^{k+1}\|\xi\|_{k+1}, \tag{9a}$$

$$\text{ii) } \|\nabla(\xi - P\xi)\| \leq Ch^{k}\|\xi\|_{k+1}, \tag{9b}$$

$$\text{iii) } \|\nabla(\xi - \Pi\xi)\| \leq Ch^{k}\|\xi\|_{k+1}. \tag{9c}$$

Lemma 2 (Skew-symmetry of the trilinear form)**.** *For ψ, $\xi \in X_h$ and $\chi \in Y_h$,*

$$b(\psi, \chi, \xi) = -b(\psi, \xi, \chi), \quad \forall \xi \in X_h. \tag{10}$$

Proof. We start from the vector identity

$$[(\nabla\psi \times \mathbf{k}) \cdot \nabla\chi]\,\xi = \nabla \cdot (\nabla\psi \times \mathbf{k})\,\chi\xi - [(\nabla\psi \times \mathbf{k}) \cdot \nabla\xi]\,\chi - \nabla \cdot [(\nabla\psi \times \mathbf{k})\,\chi\xi].$$

Integrating and using the divergence theorem, result follows because of the cyclic continuity inside an element and since $\xi \in X_h$. □

We have the following estimate for the nonlinear term.

Lemma 3. *Let $\zeta, \phi \in X$ and $\xi \in H^2 \cap X$. Then*

$$|b(\xi, \phi, \zeta)| \leq C(\Omega)\|\nabla\xi\|_1\|\nabla\phi\|\|\zeta\|_1.$$

Proof. We use Holder's inequality with $p, q = 4$ and $r = 2$. The result follows from the embedding $H^1 \hookrightarrow L^4$. □

2.1. Discrete filtering.

Definition 1. *We define the discrete Laplacian operator $\Delta_h : H_0^1 \to X^h$ in the usual way by*

$$\langle \Delta_h\psi, \chi\rangle = -\langle \nabla\psi, \nabla\chi\rangle, \ \forall \chi \in X^h. \tag{11}$$

Now we introduce the discrete filtering and the discrete deconvolution operators.

Definition 2 (Discrete filtering operator)**.** *Given $\phi \in L^2(\Omega)$, and $\alpha > 0$, the filtered $\overline{\phi}^h =: F_h\phi$ is the unique solution in X^h of*

$$\alpha^2 \left\langle \nabla\overline{\phi}^h, \nabla\xi \right\rangle + \left\langle \overline{\phi}^h, \xi \right\rangle = \langle \phi, \xi\rangle \ \ \forall \xi \in X^h. \tag{12}$$

Given $\phi \in L^2(\Omega)$, the discrete van Cittert deconvolution operator D_N^h is defined by

$$D_N^h\phi = \sum_{n=0}^{N} (I - F_h)^n\phi. \tag{13}$$

The following inequalities will be useful in the subsequent analysis.

Lemma 4. *For $\phi \in X^h$. We have the following inequalities*

$$\|D_N^h\overline{\phi}^h\| \leq N\|\phi\|_{E,0}, \tag{14}$$

$$\|I - F_h\| \leq 1, \tag{15}$$

$$\|D_N^h\phi\| \leq N\|\phi\|, \tag{16}$$

$$\|\overline{\phi}^h\| \leq \|\phi\|. \tag{17}$$

Proof. For first and second inequalities see [15]. For the third, we have

$$\|D_N^h\phi\| \leq \sum_{n=0}^{N} \|I - F_h\|^n \|\phi\| \leq N\|\phi\|, \tag{18}$$

where we use the second inequality. For the last inequality, we choose the test function equal to $\overline{\phi}^h$ in the filter equation to obtain

$$\alpha^2 \|\nabla\overline{\phi}^h\|^2 + \|\overline{\phi}^h\|^2 = \left\langle \phi, \overline{\phi}^h \right\rangle. \tag{19}$$

The result follows after applying the Cauchy-Schwarz inequality. □

Lemma 5. *The operator $D_N^h : X^h \to X^h$ is a bounded, self-adjoint positive operator. For $\phi \in X^h$,*

$$\phi = D_N^h \overline{\phi}^h + (-1)^{(N+1)} \alpha^{2N+2} \Delta_h^{N+1} F_h^{N+1} \phi. \tag{20}$$

Proof. See [15]. □

Definition 3. *As in* [15]*, we define the energy norm for the BV-α-Deconvolution model to be*

$$\|\phi\|_{E,N}^2 := \left\langle \phi, D_N^h \overline{\phi}^h \right\rangle. \tag{21}$$

With this definition we have the following equivalence between norms (see [15]).

Lemma 6. *For $\phi \in X^h$ and for each natural number N, the energy norm defined by (21) is equivalent to the zeroth order energy norm also defined by (21). That is,*

$$\|\phi\|_{E,0} \leq \|\phi\|_{E,N} \leq \sqrt{N}\|\phi\|_{E,0}. \tag{22}$$

3. Numerical scheme for BV-α-Deconvolution

Let $\phi(t^{n+\frac{1}{2}}) = \phi(({t^{n+1}} + {t^n})/2)$ for continuous variables and $\phi^{n+\frac{1}{2}} = ({\phi^{n+1}} + {\phi^n})/2$ for both the continuous and discrete variables. Based in the above variational formulation for the BV model, we define the following Crank-Nicolson type algorithm for BV-α-Deconvolution model.

Algorithm 1 (Crank-Nicolson - BV-α-Deconvolution model)**.** *Set $M = \dfrac{T}{\Delta t}$ and for n=0,...,M-1, find $(\omega^n, \psi^n, \omega^n) \in X_h \times X_h \times X_h$ satisfying:*

$$\begin{aligned} Ro\left\langle \tfrac{\omega_h^{n+1} - \omega_h^n}{\Delta t}, \lambda \right\rangle + Ro\, b\left(\psi_h^{n+\frac{1}{2}}, \omega_h^{n+\frac{1}{2}}, \lambda\right) - \left\langle \frac{\partial \psi_h^{n+\frac{1}{2}}}{\partial x}, \lambda \right\rangle \\ + \left(\tfrac{\delta_M}{L}\right)^3 \left\langle \nabla\omega_h^{n+\frac{1}{2}}, \nabla\lambda \right\rangle = \left\langle \mathcal{F}(t^{n+\frac{1}{2}}), \lambda \right\rangle \ \forall \lambda \in X^h, \end{aligned} \tag{23a}$$

$$\left\langle \nabla\psi_h^{n+1}, \nabla\chi \right\rangle = \left\langle D_N^h \overline{\omega_h^{n+1}}^h, \chi \right\rangle \ \forall \chi \in X^h, \tag{23b}$$

$$\alpha^2 \left\langle \nabla F_h \omega_h^{n+1}, \nabla\xi \right\rangle + \left\langle F_h \omega_h^{n+1}, \xi \right\rangle = \left\langle \omega_h^{n+1}, \xi \right\rangle \ \forall \xi \in X^h. \tag{23c}$$

where we assume that timestep $\Delta t > 0$, endtime $T > \Delta t$, Rossby number $Ro > 0$, Munk scale $\frac{\delta_M}{L} > 0$ and filter radius $\alpha > 0$ are given.

Now we present a lemma that will be useful in the stability analysis:

Lemma 7. *Let $(\omega_h, \psi_h) \in X^h \times X^h$ be a solution of Algorithm 1. Then we have*

$$\langle \omega_h, \psi_h \rangle = \|\nabla \psi_h\|^2 + \alpha^2 \sum_{n=0}^{N} \|(I - F_h)^{\frac{N+n}{2}} \omega_h\|^2, \tag{24}$$

$$\langle \nabla \omega_h, \nabla \psi_h \rangle = \left\langle D_N^h \overline{\omega_h}^h, \omega_h \right\rangle = \|(D_N^h F_h)^{\frac{1}{2}} \omega_h\|^2, \tag{25}$$

$$= \|D_N^h \overline{\omega_h}^h\|^2 + \alpha^2 \sum_{n=0}^{N} \|\nabla (I - F_h)^{\frac{N+n}{2}} \overline{\omega_h}^h\|^2. \tag{26}$$

Proof. Using Lemma 5 gives

$$\langle \omega_h, \psi_h \rangle = \left\langle D_N^h \overline{\omega}_h^h, \psi_h \right\rangle + (-1)^{N+1} \alpha^{2N+2} \left\langle \Delta_h^{N+1} F_h^{N+1} \omega_h, \psi_h \right\rangle. \tag{27}$$

Now, evaluating the two terms in the RHS - for the first term, we choose $\chi = \psi_h$ in (23b) to obtain

$$\|\nabla \psi_h\|^2 = \left\langle D_N^h \overline{\omega_h}, \psi_h \right\rangle. \tag{28}$$

For the second term on the RHS of (27), we rewrite (23b) using the discrete Laplacian and choose $\chi = \Delta_h^N F_h^N \overline{\omega}_h^h$ to obtain

$$-\left\langle \psi_h, \Delta_h \Delta_h^N F_h^N \overline{\omega}_h^h \right\rangle = \left\langle D_N^h \overline{\omega}_h^h, \Delta_h^N F_h^N \overline{\omega}_h^h \right\rangle. \tag{29}$$

Thus

$$-\left\langle \Delta_h^{N+1} F_h^{N+1} \omega_h, \psi_h \right\rangle = \left\langle D_N^h \overline{\omega}_h^h, \Delta_h^N F_h^N \overline{\omega}_h^h \right\rangle = \sum_{n=0}^{N} \left\langle (I - F_h)^n \overline{\omega}_h^h, \Delta_h^N F_h^N \overline{\omega}_h^h \right\rangle, \tag{30}$$

and moreover, we have

$$\Delta_h = \tfrac{-\alpha^2}{-\alpha^2} \Delta_h = -\tfrac{1}{\alpha^2} \left[\left(I - \alpha^2 \Delta_h \right) - I \right] = -\tfrac{1}{\alpha^2} \left[F_h^{-1} - I \right] = -\tfrac{1}{\alpha^2} \left[I - F_h \right] F_h^{-1}, \tag{31}$$

which implies

$$\Delta_h^N = \left(-\frac{1}{\alpha^2} \right)^N (I - F_h)^N F_h^{-N}. \tag{32}$$

Multiplying (30) by $(-1)^N \alpha^{2N}$ and applying (32) produces

$$\begin{aligned} (-1)^{N+1} \alpha^{2N} \left\langle \Delta_h^{N+1} F_h^{N+1} \omega_h, \psi_h \right\rangle &= \sum_{n=0}^{N} \left\langle (I - F_h)^n \overline{\omega}_h^h, (I - F_h)^N \overline{\omega}_h^h \right\rangle \\ &= \sum_{n=0}^{N} \|(I - F_h)^{\frac{N+n}{2}} \overline{\omega}_h^h\|^2. \end{aligned}$$

(24) follows after we use the above equation multiplied by α^2.

Now, we prove (25) and (26). (25) follows from (23b) with $\chi = \omega_h$ because F_h and D_N^h are self-adjoint and positive [15]. For (26), we use (32) and Lemma (5) to obtain

$$\omega_h = D_N^h \overline{\omega_h}^h + (I - F_h)^{N+1} \omega_h. \tag{33}$$

Thus, using (23b) with $\chi = \omega_h$,the definition of D_N^h results and as F_h is self-adjoint and positive results

$$\begin{aligned}\langle \nabla\psi_h, \nabla\omega_h\rangle &= \left\langle D_N^h\overline{\omega_h}^h, \omega_h\right\rangle = \left\langle D_N^h\overline{\omega_h}^h, D_N^h\overline{\omega_h}^h\right\rangle + \left\langle D_N^h\overline{\omega_h}^h, (I-F_h)^{N+1}\,\omega_h\right\rangle \\ &= \|D_N^h\overline{\omega_h}^h\|^2 + \sum_{n=0}^{N}\left\langle (I-F_h)^n\,\overline{\omega_h}^h, (I-F_h)^N\,(I-F_h)\,\omega_h\right\rangle \\ &= \|D_N^h\overline{\omega_h}^h\|^2 + \sum_{n=0}^{N}\left\langle (I-F_h)^{\frac{N+n}{2}}\,\overline{\omega_h}^h, (I-F_h)\,(I-F_h)^{\frac{N+n}{2}}\,\omega_h\right\rangle.\end{aligned}$$

Finally, applying the filter equation to $(I-F_h)^{\frac{N+n}{2}}\omega_h$, choosing the test function to be $(I-F_h)^{\frac{N+n}{2}}\overline{\omega_h}^h$, and using the fact that $(I-F_h)^{\frac{N+n}{2}}$ commutes with F_h, we obtain

$$\alpha^2\|\nabla(I-F_h)^{\frac{N+n}{2}}\overline{\omega_h}^h\| = \left\langle (I-F_h)(I-F_h)^{\frac{N+n}{2}}\omega_h, (I-F_h)^{\frac{N+n}{2}}\overline{\omega_h}^h\right\rangle$$

from which we have

$$\begin{aligned}\langle \nabla\psi_h, \nabla\omega_h\rangle &= \|D_N^h\overline{\omega_h}^h\|^2 + \alpha^2\sum_{n=0}^{N}\left\langle \nabla\,(I-F_h)^{\frac{N+n}{2}}\,\overline{\omega_h}^h, \nabla F_h\,(I-F_h)^{\frac{N+n}{2}}\,\omega_h\right\rangle \\ &= \|D_N^h\overline{\omega_h}^h\|^2 + \alpha^2\sum_{n=0}^{N}\|\nabla(I-F_h)^{\frac{N+n}{2}}\overline{\omega_h}^h\|^2,\end{aligned}$$

□

Thus, we define the modified BV-α-Deconvolution kinetic energy, energy dissipation and enstrophy respectively as:

$$E_\alpha^N(\psi,\omega) := \tfrac{1}{2}\langle\psi,\omega\rangle = \tfrac{1}{2}\|\nabla\psi\|^2 + \tfrac{1}{2}\alpha^2\sum_{n=0}^{N}\|(I-F_h)^{\frac{N+n}{2}}\overline{\omega}^h\|^2, \tag{34}$$

$$\begin{aligned}\epsilon_\alpha^N(\omega) &:= \left(\tfrac{\delta_M}{L}\right)^3\langle\nabla\psi,\nabla\omega\rangle = \left(\tfrac{\delta_M}{L}\right)^3\|D_N^h\overline{\omega}^h\|^2 \\ &\quad + \left(\tfrac{\delta_M}{L}\right)^3\alpha^2\sum_{n=0}^{N}\|\nabla(I-F_h)^{\frac{N+n}{2}}\overline{\omega}^h\|^2,\end{aligned} \tag{35}$$

$$\mathcal{E}(\omega) := \tfrac{1}{2}\|\omega\|^2. \tag{36}$$

Remark 1. *Due to linearity of equation (23b), in both F_h and D_N^h we have*

$$\left\langle \omega^{n+1}-\omega^n, \psi^{n+\frac{1}{2}}\right\rangle = E_\alpha^N(\psi_h^{n+1},\omega_h^{n+1}) - E_\alpha^N(\psi_h^n,\omega_h^n).$$

Lemma 8 (Conservation of Kinetic Energy)**.** *The BV-α-Deconvolution model solution satisfies*

$$E_\alpha^N(\psi_h^M,\omega_h^M) + \frac{\Delta t}{Ro}\sum_{n=0}^{M-1}\epsilon_\alpha^N(\omega_h^{n+\frac{1}{2}}) = E_\alpha^N(\psi_h^0,\omega_h^0) + \frac{\Delta t}{Ro}\sum_{n=0}^{M-1}\left\langle \mathcal{F}(t^{n+\frac{1}{2}}), \psi_h^{n+\frac{1}{2}}\right\rangle.$$

In particular, if $\delta_M = 0$ and $\mathcal{F} = 0$ we have $E_\alpha^N(\psi_h^M,\omega_h^M) = E_\alpha^N(\psi_h^0,\omega_h^0)$.

Proof. We rewrite the nonlinear term in (23a) as $b(\psi_h^{n+\frac{1}{2}}, Ro\,\omega_h^{n+\frac{1}{2}}+y, \lambda)$ and choose $\lambda = \psi_h^{n+\frac{1}{2}}$. We obtain, after we use the definition of modified energy and dissipation and the skew-symmetry of the trilinear form,

$$E_\alpha^N(\psi_h^{n+1},\omega_h^{n+1}) - E_\alpha^N(\psi_h^n,\omega_h^n) + \frac{\Delta t}{Ro}\epsilon_N^\alpha(\omega_h^{n+\frac{1}{2}}) = \left\langle \mathcal{F}(t^{n+\frac{1}{2}}), \psi_h^{n+\frac{1}{2}} \right\rangle. \tag{37}$$

The result follows after we sum from $n = 0, ..., M-1$. □

Algorithm 1 also conserves enstrophy.

Lemma 9 (Conservation of enstrophy)**.** *The BV-α-Deconvolution model solution satisfies*

$$\begin{aligned}\|\mathcal{E}(\omega_h^M)\| + \tfrac{\Delta t}{Ro}\left(\tfrac{\delta_M}{L}\right)^3 \sum_{n=0}^{M} \left\|\nabla\omega_h^{n+\frac{1}{2}}\right\|^2 = \\ \|\mathcal{E}(\omega_h^0)\| + \tfrac{\Delta t}{Ro}\sum_{n=0}^{M}\left\langle \tfrac{\partial\psi_h^{n+\frac{1}{2}}}{\partial x}, \omega_h^{n+\frac{1}{2}}\right\rangle + \tfrac{\Delta t}{Ro}\sum_{n=0}^{M}\left\langle \mathcal{F}(t^{n+\frac{1}{2}}), \omega_h^{n+\frac{1}{2}}\right\rangle.\end{aligned} \tag{38}$$

In particular, if $\delta_M = \mathcal{F} = 0$ and $Ro \to \infty$, $\|\mathcal{E}(\omega_h^M)\| = \|\mathcal{E}(\omega_h^0)\|$.

Proof. Choosing $\lambda = \omega_h^{n+\frac{1}{2}} = \frac{1}{2}(\omega_h^{n+1} + \omega_h^n)$ in (23a), using the skew-symmetry of the trilinear term, the enstrophy definition, and multiplying by $\dfrac{\Delta t}{Ro}$ gives

$$\begin{aligned}&\|\mathcal{E}(\omega_h^{n+1})\| + \tfrac{\Delta t}{Ro}\left(\tfrac{\delta_M}{L}\right)^3\|\nabla\omega_h^{n+\frac{1}{2}}\|^2 \\ =&\|\mathcal{E}(\omega_h^n)\| + \tfrac{\Delta t}{Ro}\left\langle \frac{\partial\psi_h^{n+\frac{1}{2}}}{\partial x}, \omega_h^{n+\frac{1}{2}}\right\rangle + \tfrac{\Delta t}{Ro}\left\langle \mathcal{F}(t^{n+\frac{1}{2}}), \omega_h^{n+\frac{1}{2}}\right\rangle.\end{aligned} \tag{39}$$

The result now follows after we sum from $n = 0, ..., M-1$. □

Lemma 10 (Stability)**.** *Algorithm 1 is unconditionally stable. Its solutions satisfy*

(40)

$$Ro\|\nabla\psi_h^M\|^2 + Ro\tfrac{\alpha^2}{2}\sum_{n=0}^{N}\|(I-F_h)^{\frac{N+M}{2}}\overline{\omega}\|^2 + \tfrac{\Delta t}{2N}\left(\tfrac{\delta_M}{L}\right)^3\sum_{n=0}^{M}\|\Delta_h\psi_h^{n+\frac{1}{2}}\|^2 \le C(data),$$

$$\|\omega_h^M\|^2 + \tfrac{\Delta t}{2Ro}\left(\tfrac{\delta_M}{L}\right)^3\textstyle\sum_{n=0}^{M}\left\|\nabla\omega_h^{n+\frac{1}{2}}\right\|^2 \le C(data). \tag{41}$$

Remark 2. *The bounds* (40)-(41) *are sufficient for the Leray-Schauder fixed point theorem to be applied, in order to prove existence of a solution at each timestep (as in* [11]*). Uniqueness can be proven in the standard way, and will hold provided a timestep restriction.*

Proof. For any $\Delta t > 0$ we start with the estimate (40). First, note that using the definition of the discrete Laplacian, equation (23b), choosing $\chi = \Delta_h\psi_h^{n+\frac{1}{2}}$ and using Cauchy-Schwarz yields:

$$\|\Delta_h\psi_h^{n+\frac{1}{2}}\| \le \|D_N^h\overline{\omega_h^{n+\frac{1}{2}}}^h\|. \tag{42}$$

Now using Lemma 4 and norm equivalence in Lemma 6

$$\|\Delta_h \psi_h^{n+\frac{1}{2}}\| \leq N\|\omega_h^{n+\frac{1}{2}}\|_{E,N} = N\left\langle D_N^h \overline{\omega_h^{n+\frac{1}{2}}}^h, \omega_h^{n+\frac{1}{2}} \right\rangle$$

$$= N\left\langle \nabla\psi_h^{n+\frac{1}{2}}, \nabla\omega_h^{n+\frac{1}{2}} \right\rangle. \tag{43}$$

Using inequality (43), equation (37) and Cauchy-Schwarz inequality we obtain

$$E_\alpha^N(\psi_h^{n+1}, \omega_h^{n+1}) - E_\alpha^N(\psi_h^n, \omega_h^n) + \tfrac{\Delta t}{NRo}\left(\tfrac{\delta_M}{L}\right)^3 \|\Delta_h \psi_h^{n+\frac{1}{2}}\|$$

$$\leq \tfrac{\Delta t}{Ro}\|\mathcal{F}(t^{n+\frac{1}{2}})\|_{-1}\|\nabla\psi_h^{n+\frac{1}{2}}\|. \tag{44}$$

Averaging the definition of modified Laplacian and choosing $\chi = \psi_h^{n+\frac{1}{2}}$ we find

$$\|\nabla\psi_h^{n+\frac{1}{2}}\| \leq C_{PF}\|\Delta_h\psi_h^{n+\frac{1}{2}}\|. \tag{45}$$

Then we obtain estimate (40) using (45) in (44), Young's inequality with $\epsilon = \left(\frac{L}{\delta_M}\right)^3$ and summing from $n = 0, ..., M-1$.

For estimate (41), we use (39), Cauchy-Schwarz and Young's inequalities and the definition of enstrophy. Summing from $n = 0, ..., M-1$ finishes the proof. □

4. Convergence

The following lemma is the key to handling the consistency error in the BV-α-Deconvolution model.

Lemma 11. *For smooth, periodic ϕ, or ϕ satisfying $\Delta^j\phi = 0$ on $\partial\Omega$ for $0 \leq j \leq \dfrac{k+1}{2} - 1$, the discrete approximate deconvolution operator satisfies*

$$\|\phi - D_N^h\overline{\phi}^h\| \leq C\alpha^{2N+2}\|\Delta^{N+1}F^{N+1}\phi\| + C(\alpha h^k + h^{k+1})\left(\sum_{n=0}^{N+1}|F^n\phi|_{k+1}\right), \tag{46}$$

and thus for $k \geq 1$ we have

$$\|\phi - D_N^h\overline{\phi}^h\| \leq C(\alpha^{2N+2} + \alpha h^k + h^{k+1})\left(\sum_{n=0}^{N+1}|F^n\phi|_{k+1}\right). \tag{47}$$

Proof. See [12]. □

Theorem 1 (Convergence)**.** *Consider the discrete BV-α-Deconvolution model. Let $(\omega(t), \psi(t)) \in X_h \times X_h$ be a smooth strong solution of the BV model satisfying free slip boundary conditions such that the norms of $(\omega(t), \psi(t))$ on the right hand side of (48) and (49) are finite. Suppose ω_h, ψ_h solves the Crank-Nicolson approximation (23a)-(23c) of the BV-α-Deconvolution model. Then for Δt small enough (in order to apply the discrete Gronwall inequality), we have*

$$|||\omega - \omega_h|||_{\infty,0} \leq f(\Delta t, h, \alpha) + Ch^{k+1}\,|||\omega|||_{\infty,k+1}, \tag{48}$$

$$\left(\left(\tfrac{\delta_M}{L}\right)^3\sum_{n=0}^{M-1}\Delta t\left\|\nabla\left(\omega(t^{n+\frac{1}{2}}) - \omega_h^{n+\frac{1}{2}}\right)\right\|^2\right)^{1/2} \leq f(\Delta t, h, \alpha) + C\Delta t^2\left(\tfrac{\delta_M}{L}\right)^{3/2}\|\omega_{tt}\|_{2,0}$$

$$+ C\left(\frac{\delta_M}{L}\right)^{3/2} h^k\,|||\omega|\,||_{2,k+1}, \tag{49}$$

where

$$
\begin{aligned}
f(\Delta t,h,\alpha) :=& C^*\Big\{h^k\Big[\tfrac{C}{Ro^{\frac{1}{2}}}\left(\tfrac{\delta_M}{L}\right)^{\frac{3}{2}}|||\omega|||_{2,k+1}+\tfrac{C}{Ro^{\frac{1}{2}}}\left(\tfrac{L}{\delta_M}\right)^{\frac{3}{2}}|||\psi|||_{2,k+1}\\
&+h\tfrac{C}{Ro^{\frac{1}{2}}}\left(\tfrac{L}{\delta_M}\right)^{\frac{3}{2}}|||\omega|||_{2,k+1}+C(\tfrac{L}{\delta_M})^{\frac{3}{2}}|||\nabla\omega|||^2_{4,1}+C(\tfrac{L}{\delta_M})^{\frac{3}{2}}|||\psi|||^2_{4,k+1}\\
&+hC(\tfrac{L}{\delta_M})^{\frac{3}{2}}|||\omega|||^2_{4,k+1}+hC\left(\tfrac{L}{\delta_M}\right)^{\frac{3}{2}}|||\psi|||^2_{4,k+1}\Big]\\
&+C(\alpha^{2N+2}+\alpha h^k+h^{k+1})\Big[\sum_{n=0}^{N+1}|||F^n\omega|||_{2,k+1}+\left(\tfrac{L}{\delta_M}\right)^{\frac{3}{2}}|||\nabla\omega|||^2_{4,1}\\
&+\left(\tfrac{L}{\delta_M}\right)^{\frac{3}{2}}\sum_{n=0}^{N+1}|||F^n\omega|||^2_{4,k+1}+\left(\tfrac{L}{\delta_M}\right)^{\frac{3}{2}}|||\omega|||^2_{4,k+1}\Big]+\Delta t^2\Big[(\tfrac{L}{\delta_M})^{\frac{3}{2}}C\|\omega_{ttt}\|_{2,0}\\
&+C\left(\tfrac{\delta_M}{L}\right)^{\frac{3}{2}}\|\nabla\omega_{tt}\|_{2,0}+C\left(\tfrac{L}{\delta_M}\right)^{\frac{3}{2}}\|\psi_{tt}\|_{2,0}+C\left(\tfrac{L}{\delta_M}\right)^{\frac{3}{2}}|||\nabla\psi^{\frac{1}{2}}|||^2_{4,1}\\
&+C\left(\tfrac{L}{\delta_M}\right)^{\frac{3}{2}}\|\omega_{tt}\|^2_{4,1}+C\left(\tfrac{L}{\delta_M}\right)^{\frac{3}{2}}|||\nabla\omega|||^2_{4,1}+C\left(\tfrac{L}{\delta_M}\right)^{\frac{3}{2}}\|\psi_{tt}\|^2_{4,1}\Big]\Big\}.
\end{aligned}
\tag{50}
$$

Corollary 1. *Suppose that the indicated norms on the right hand side of (48)-(50) are finite. Then the error in the Crank-Nicolson finite element scheme for the BV-α-deconvolution is of the order*

$$
\begin{aligned}
|||\omega-\omega_h|||_{\infty,0}+\left(\left(\tfrac{\delta_M}{L}\right)^3\sum_{n=0}^{M-1}\Delta t\|\nabla(\omega(t^{n+\frac{1}{2}})-\omega_h^{n+\frac{1}{2}})\|^2\right)^{1/2}\\
\leq O\left(h^k+\Delta t^2+\alpha^{2N+2}\sum_{n=0}^{N+1}|||F^n\omega|||_{2,k+1}\right).
\end{aligned}
$$

Moreover,

$$
|||\psi-\psi_h|||_{2,1}\leq O\left(h^k+\Delta t^2+\alpha^{2N+2}\sum_{n=0}^{N+1}|||F^n\omega|||_{2,k+1}\right).
\tag{51}
$$

Proof of Theorem 1. The BV model solution satisfies

$$
\begin{aligned}
&Ro\left\langle\tfrac{\omega^{n+1}-\omega^n}{\Delta t},v_h\right\rangle+Ro\,b\left(\psi^{n+\frac{1}{2}},\omega^{n+\frac{1}{2}},v_h\right)-\left\langle\tfrac{\partial\psi^{n+\frac{1}{2}}}{\partial x},v_h\right\rangle+\left(\tfrac{\delta_M}{L}\right)^3\left\langle\nabla\omega^{n+\frac{1}{2}},\nabla v_h\right\rangle\\
&\qquad=\left\langle\mathcal{F}(t^{n+\frac{1}{2}}),v_h\right\rangle+Intp(\omega^n,\psi^n;v_h)\ \forall v_h\in X^h,
\end{aligned}
\tag{52}
$$

where

$$
\begin{aligned}
Intp(\omega^n,\psi^n;v_h) :=& Ro\left\langle\tfrac{\omega^{n+1}-\omega^n}{\Delta t}-\omega_t(t^{n+\frac{1}{2}}),v_h\right\rangle+\left(\tfrac{\delta_M}{L}\right)^3\left\langle\nabla\omega^{n+\frac{1}{2}}-\nabla\omega(t^{n+\frac{1}{2}}),\nabla v_h\right\rangle\\
&-\left\langle\frac{\partial\psi^{n+\frac{1}{2}}}{\partial x}-\frac{\partial\psi(t^{n+\frac{1}{2}})}{\partial x},v_h\right\rangle+Ro\left[b\left(\psi^{n+\frac{1}{2}},\omega^{n+\frac{1}{2}},v_h\right)-b\left(\psi(t^{n+\frac{1}{2}}),\omega(t^{n+\frac{1}{2}}),v_h\right)\right].
\end{aligned}
\tag{53}
$$

We define the vorticity and streamfunction error as

$$
e:=\omega-\omega_h=(\omega-P\omega)-(\omega_h-P\omega)=e_\perp-e_h,
\tag{54a}
$$

$$
E:=\psi-\psi_h=(\psi-\Pi\psi)-(\psi_h-\Pi\psi)=E_\perp-E_h.
\tag{54b}
$$

Now we subtract (23a) from (52), add $\pm b\left(\psi_h^{n+\frac{1}{2}}, \omega^{n+\frac{1}{2}}, v_h\right)$ and fix $v_h = e_h^{n+\frac{1}{2}}$

$$\begin{aligned}
&\|e_h^{n+1}\|^2 - \|e_h^n\|^2 + \frac{2\Delta t}{Ro}\left(\tfrac{\delta_M}{L}\right)^3\|\nabla e_h^{n+\frac{1}{2}}\|^2 = \tfrac{2\Delta t}{Ro}\left(\tfrac{\delta_M}{L}\right)^3\left\langle \nabla e_\perp^{n+\frac{1}{2}}, \nabla e_h^{n+\frac{1}{2}}\right\rangle \\
&-\frac{2\Delta t}{Ro}\left\langle \frac{\partial E^{n+\frac{1}{2}}}{\partial x}, e_h^{n+\frac{1}{2}}\right\rangle + 2\Delta t\left[b\left(\psi_h^{n+\frac{1}{2}}, e_\perp^{n+\frac{1}{2}}, e_h^{n+\frac{1}{2}}\right) + b\left(E^{n+\frac{1}{2}}, \omega^{n+\frac{1}{2}}, e_h^{n+\frac{1}{2}}\right)\right] \\
&-\frac{2\Delta t}{Ro} Intp(\omega^n, \psi^n; e_h^{n+\frac{1}{2}}), \qquad (55)
\end{aligned}$$

because $\left\langle e_\perp^{n+1} - e_\perp^n, e_h^{n+\frac{1}{2}}\right\rangle = 0$ and $b\left(\psi_h^{n+\frac{1}{2}}, e_h^{n+\frac{1}{2}}, e_h^{n+\frac{1}{2}}\right) = 0$.

The next step is to bound the RHS terms in (55). The term below is bounded in a standard way using Cauchy-Schwarz and Young inequalities and Lemma 1.

$$\left|\left(\tfrac{\delta_M}{L}\right)^3\left\langle \nabla e_\perp^{n+\frac{1}{2}}, \nabla e_h^{n+\frac{1}{2}}\right\rangle\right| \le \frac{1}{16}\left(\tfrac{\delta_M}{L}\right)^3\|\nabla e_h^{n+\frac{1}{2}}\|^2 + Ch^{2k}\left(\tfrac{\delta_M}{L}\right)^3\|\omega^{n+\frac{1}{2}}\|_{k+1}^2. \qquad (56)$$

Using Poincaré and Young inequalities with $\epsilon = \frac{1}{8}\left(\frac{\delta_M}{L}\right)^3$ we obtain

$$\left|\left\langle \frac{\partial E^{n+\frac{1}{2}}}{\partial x}, e_h^{n+\frac{1}{2}}\right\rangle\right| \le \frac{1}{16}\left(\tfrac{\delta_M}{L}\right)^3\|\nabla e_h^{n+\frac{1}{2}}\|^2 + C\left(\tfrac{L}{\delta_M}\right)^3\|\nabla E^{n+\frac{1}{2}}\|^2. \qquad (57)$$

Now we have to estimate the term $\|\nabla E^{n+\frac{1}{2}}\|$. Averaging and subtracting (5b) from (23b), choosing $v_h = E_h^{n+\frac{1}{2}}$ and using Cauchy-Schwarz and Poincaré inequalities, we obtain

$$\|\nabla E_h^{n+\frac{1}{2}}\|^2 \le C\|D_N^h\overline{(\omega_h^{n+\frac{1}{2}} - \omega^{n+\frac{1}{2}})}^h\|\|\nabla E_h^{n+\frac{1}{2}}\| + C\|D_N^h\overline{\omega^{n+\frac{1}{2}}}^h - \omega^{n+\frac{1}{2}}\|\|\nabla E_h^{n+\frac{1}{2}}\|. \qquad (58)$$

Using (58) and Lemma 4 we obtain

$$\|\nabla E^{n+\frac{1}{2}}\|^2 \le \|\nabla E_\perp^{n+\frac{1}{2}}\|^2 + C\|e_h^{n+\frac{1}{2}}\|^2 + C\|e_\perp^{n+\frac{1}{2}}\|^2 + C\|D_N^h\overline{\omega^{n+\frac{1}{2}}}^h - \omega^{n+\frac{1}{2}}\|^2. \qquad (59)$$

Using (59) and Lemmas 1 and 11

$$\begin{aligned}
&\left|\left\langle \frac{\partial E^{n+\frac{1}{2}}}{\partial x}, e_h^{n+\frac{1}{2}}\right\rangle\right| \le \frac{1}{16}\left(\tfrac{\delta_M}{L}\right)^3\|\nabla e_h^{n+\frac{1}{2}}\|^2 \\
&+ C\left(\tfrac{L}{\delta_M}\right)^3\left(C\|\nabla E_\perp^{n+\frac{1}{2}}\|^2 + C\|e_\perp^{n+\frac{1}{2}}\|^2 + C\|e_h^{n+\frac{1}{2}}\|^2 + C\|D_N^h\overline{\omega^{n+\frac{1}{2}}}^h - \omega^{n+\frac{1}{2}}\|^2\right) \\
&\le \frac{1}{16}\left(\tfrac{\delta_M}{L}\right)^3\|\nabla e_h^{n+\frac{1}{2}}\|^2 + C\left(\tfrac{L}{\delta_M}\right)^3\|e_h^{n+\frac{1}{2}}\|^2 + \left(\tfrac{L}{\delta_M}\right)^3\Big[Ch^{2k}\|\psi^{n+\frac{1}{2}}\|_{k+1}^2 \\
&+Ch^{2k+2}\|\omega^{n+\frac{1}{2}}\|_{k+1}^2 + C(\alpha^{4N+4} + \alpha^2h^{2k} + h^{2k+2})\left(\sum_{n=0}^{N+1}|F^n\omega^{n+\frac{1}{2}}|_{k+1}\right)\Big]. \qquad (60)
\end{aligned}$$

For the first trilinear term we use Lemma 3, Young inequality with $\epsilon = \frac{1}{8Ro}\left(\frac{\delta_M}{L}\right)^3$, Poincaré inequality, (59), Lemmas 1 and 11 and as $k \geq 1$ we have

$$\begin{aligned}
&\left|b\left(E^{n+\frac{1}{2}}, \omega^{n+\frac{1}{2}}, e_h^{n+\frac{1}{2}}\right)\right| \leq \frac{1}{16}\left(\tfrac{\delta_M}{L}\right)^3 \|\nabla e_h^{n+\frac{1}{2}}\|^2 + C\left(\tfrac{L}{\delta_M}\right)^3 \|\nabla \omega^{n+\frac{1}{2}}\|_1^2 \|\nabla E^{n+\frac{1}{2}}\|^2 \\
&\leq \frac{1}{16}\left(\tfrac{\delta_M}{L}\right)^3 \|\nabla e_h^{n+\frac{1}{2}}\|^2 + C\left(\tfrac{L}{\delta_M}\right)^3 \|\nabla \omega^{n+\frac{1}{2}}\|_1^2 \|e_h^{n+\frac{1}{2}}\|^2 \\
&+ \left(\tfrac{L}{\delta_M}\right)^3 \|\nabla \omega^{n+\frac{1}{2}}\|_1^2 \left(Ch^{2k}\|\psi^{n+\frac{1}{2}}\|_{k+1}^2 + Ch^{2k+2}\|\omega^{n+\frac{1}{2}}\|_{k+1}^2 + C\|D_N^h \overline{\omega^{n+\frac{1}{2}}}^h - \omega^{n+\frac{1}{2}}\|^2\right) \\
&\leq \frac{1}{16}\left(\tfrac{\delta_M}{L}\right)^3 \|\nabla e_h^{n+\frac{1}{2}}\|^2 + C\left(\tfrac{L}{\delta_M}\right)^3 \|\nabla \omega^{n+\frac{1}{2}}\|_1^2 \|e_h^{n+\frac{1}{2}}\|^2 \\
&+ C\left(\tfrac{L}{\delta_M}\right)^3 h^{2k}(\|\nabla \omega^{n+\frac{1}{2}}\|_1^4 + \|\psi^{n+\frac{1}{2}}\|_{k+1}^4) + C\left(\tfrac{L}{\delta_M}\right)^3 Ch^{2k+2}\|\omega^{n+\frac{1}{2}}\|_{k+1}^4 \\
&+ C\left(\tfrac{L}{\delta_M}\right)^3 (\alpha^{4N+4} + \alpha^2 h^{2k} + h^{2k+2})\left(\|\nabla \omega^{n+\frac{1}{2}}\|_1^4 + \left(\sum_{n=0}^{N+1} |F^n \omega^{n+\frac{1}{2}}|_{k+1}^4\right)\right).
\end{aligned} \tag{61}$$

Using Holder's inequality with $p = \infty$ and $q = r = 2$,

$$\left|b\left(\psi_h^{n+\frac{1}{2}}, e_\perp^{n+\frac{1}{2}}, e_h^{n+\frac{1}{2}}\right)\right| \leq \|\nabla \psi_h^{n+\frac{1}{2}}\|_\infty \|e_\perp^{n+\frac{1}{2}}\|^2 \|\nabla e_h^{n+\frac{1}{2}}\|^2.$$

From $\|\nabla \psi_h^{n+\frac{1}{2}} - \nabla \psi^{n+\frac{1}{2}}\|_\infty = \|\nabla E^{n+\frac{1}{2}}\|_\infty$ and using the embedding $L^\infty \hookrightarrow H^2$ and the regularity estimate for elliptic equations

$$\begin{aligned}
\|\nabla \psi_h^{n+\frac{1}{2}}\|_\infty &\leq \|\nabla E^{n+\frac{1}{2}}\|_\infty + \|\nabla \psi^{n+\frac{1}{2}}\|_\infty \leq \|\nabla E^{n+\frac{1}{2}}\|_\infty + C\|\psi^{n+\frac{1}{2}}\|_3 \\
&\leq \|\nabla E^{n+\frac{1}{2}}\|_\infty + C\|\omega^{n+\frac{1}{2}}\|_1.
\end{aligned} \tag{62}$$

Now we have to estimate the term $\|\nabla E^{n+\frac{1}{2}}\|_\infty$ in the above inequality. Let I^h be a global Lagrangian interpolator, we have $\|\nabla E^{n+\frac{1}{2}}\|_\infty \leq \|\nabla(I^h \psi^{n+\frac{1}{2}} - \psi_h^{n+\frac{1}{2}})\|_\infty + \|\nabla(\psi^{n+\frac{1}{2}} - I^h \psi^{n+\frac{1}{2}})\|_\infty$. Using an inverse inequality for $\|\nabla(I^h \psi^{n+\frac{1}{2}} - \psi_h^{n+\frac{1}{2}})\|_\infty$ (Theorem 4.5.11 in [2]) and a standard estimate for $\|\nabla(\psi^{n+\frac{1}{2}} - I^h \psi^{n+\frac{1}{2}})\|_\infty$ (estimate (4.4.22) of Theorem 4.4.20 in [2] with $p = 2$, $n = 2$, $s = 1$ and $m = k+1$) we have

$$\begin{aligned}
\|\nabla E^{n+\frac{1}{2}}\|_\infty &\leq Ch^{-1}\|\nabla(I^h \psi^{n+\frac{1}{2}} - \psi_h^{n+\frac{1}{2}})\| + Ch^{k-1}\|\psi^{n+\frac{1}{2}}\|_{k+1} \\
&\leq Ch^{-1}\|\nabla(I^h \psi^{n+\frac{1}{2}} - \psi^{n+\frac{1}{2}} - E^{n+\frac{1}{2}})\| + Ch^{k-1}\|\psi^{n+\frac{1}{2}}\|_{k+1} \\
&\leq Ch^{-1}\|\nabla E_h^{n+\frac{1}{2}}\| + Ch^{k-1}\|\psi^{n+\frac{1}{2}}\|_{k+1}.
\end{aligned} \tag{63}$$

Thus, for $0 < h \leq 1$ and for $k \geq 1$ we have

$$\|\nabla \psi_h^{n+\frac{1}{2}}\|_\infty \leq Ch^{-1}\|\nabla E_h^{n+\frac{1}{2}}\| + C\|\omega^{n+\frac{1}{2}}\|_1 + C\|\psi^{n+\frac{1}{2}}\|_{k+1}.$$

Therefore, for $0 < h \leq 1$ and $k \geq 1$ and using Lemma 1

$$\begin{aligned}
\left|b\left(\psi_h^{n+\frac{1}{2}}, e_\perp^{n+\frac{1}{2}}, e_h^{n+\frac{1}{2}}\right)\right| &\leq \left(Ch^{-1}\|\nabla E_h^{n+\frac{1}{2}}\| + \|\omega^{n+\frac{1}{2}}\|_1 + \|\psi^{n+\frac{1}{2}}\|_{k+1}\right)\|e_\perp^{n+\frac{1}{2}}\|\|\nabla e_h^{n+\frac{1}{2}}\| \\
&\leq C\|\omega^{n+\frac{1}{2}}\|_{k+1}\|\nabla E_h^{n+\frac{1}{2}}\|\|\nabla e_h^{n+\frac{1}{2}}\| \\
&+ C\left(\|\omega^{n+\frac{1}{2}}\|_1 + \|\psi^{n+\frac{1}{2}}\|_{k+1}\right)\|e_\perp^{n+\frac{1}{2}}\|\|\nabla e_h^{n+\frac{1}{2}}\|.
\end{aligned}$$

Using Young inequality in both terms with $\epsilon = \dfrac{1}{16CRo}\left(\frac{\delta_M}{L}\right)^3$, (58), $k \geq 1$ and Lemma 1

$$
\begin{aligned}
&\left| b\left(\psi_h^{n+\frac{1}{2}}, e_\perp^{n+\frac{1}{2}}, e_h^{n+\frac{1}{2}}\right)\right| \leq \frac{1}{16}\left(\tfrac{\delta_M}{L}\right)^3 \|\nabla e_h^{n+\frac{1}{2}}\|^2 + 8\left(\tfrac{L}{\delta_M}\right)^3 \|\psi^{n+\frac{1}{2}}\|_{k+1}^2 \|e_\perp^{n+\frac{1}{2}}\|^2 \\
&+ 8\left(\tfrac{L}{\delta_M}\right)^3 \|\omega^{n+\frac{1}{2}}\|_{k+1}^2 \left(C\|e_\perp^{n+\frac{1}{2}}\|^2 + C\|e_h^{n+\frac{1}{2}}\|^2 + C\|D_N^h \overline{\omega^{n+\frac{1}{2}}}^h - \omega^{n+\frac{1}{2}}\|^2 + C\|e_\perp^{n+\frac{1}{2}}\|^2 \right) \\
&\leq \frac{1}{16}\left(\tfrac{\delta_M}{L}\right)^3 \|\nabla e_h^{n+\frac{1}{2}}\|^2 + C\left(\tfrac{L}{\delta_M}\right)^3 \|\omega^{n+\frac{1}{2}}\|_{k+1}^2 \|e_h^{n+\frac{1}{2}}\|^2 \\
&+ \left(\tfrac{L}{\delta_M}\right)^3 \Big[Ch^{2k+2} \|\psi^{n+\frac{1}{2}}\|_{k+1}^4 + \left(\alpha^{4N+4} + \alpha^2 h^{2k} + Ch^{2k+2}\right) \|\omega^{n+\frac{1}{2}}\|_{k+1}^4 \\
&+ C(\alpha^{4N+4} + \alpha^2 h^{2k} + h^{2k+2}) \left(\sum_{n=0}^{N+1} |F^n \omega^{n+\frac{1}{2}}|_{k+1}^4 \right) \Big].
\end{aligned}
\tag{64}
$$

It remains to bound the term $Intp$. Standard analysis for the interpolation error (see, e.g., [13] and [15]) gives

$$
\begin{aligned}
&\sum_{n=0}^{M-1} \Delta t \left| Intp(\omega^n, \overline{\psi^n}^h; e_h^{n+\frac{1}{2}}) \right| \leq \sum_{n=0}^{M-1} \frac{\Delta t}{4}\left(\tfrac{\delta_M}{L}\right)^3 \left\| \nabla e_h^{n+\frac{1}{2}} \right\|^2 + CRo^2 \left(\tfrac{L}{\delta_M}\right)^3 \Delta t^4 \|\omega_{ttt}\|_{2,0}^2 \\
&+ C\left(\tfrac{\delta_M}{L}\right)^3 \Delta t^4 \|\nabla \omega_{tt}\|_{2,0}^2 + C\left(\tfrac{L}{\delta_M}\right)^3 \Delta t^4 \|\psi_{tt}\|_{2,0}^2 + C\Delta t^4 \left(\tfrac{L}{\delta_M}\right)^3 \left\| \nabla \psi^{1/2} \right\|_{4,1}^4 \\
&+ C\Delta t^4 \left(\tfrac{L}{\delta_M}\right)^3 \|\omega_{tt}\|_{4,1}^4 + C\Delta t^4 \left(\tfrac{\delta_M}{L}\right)^3 \left\| \nabla \omega^{1/2} \right\|_{4,1}^4 + C\Delta t^4 \left(\tfrac{L}{\delta_M}\right)^3 \|\psi_{tt}\|_{4,1}^4.
\end{aligned}
\tag{65}
$$

Now, using (56), (60), (61), (64) in (55), summing from $n = 0$ to $n = M-1$ and using (65) we obtain

$$
\begin{aligned}
&\|e_h^M\|^2 - \|e_h^0\|^2 + \tfrac{\Delta t}{Ro}\left(\tfrac{\delta_M}{L}\right)^3 \sum_{n=0}^{M-1} \|\nabla e_h^{n+\frac{1}{2}}\|^2 \leq h^{2k} \tfrac{C}{Ro}\left(\tfrac{\delta_M}{L}\right)^3 |||\omega|||_{2,k+1}^2 \\
&+ h^{2k} \tfrac{C}{Ro}\left(\tfrac{L}{\delta_M}\right)^3 |||\psi|||_{2,k+1}^2 + h^{2k+2} \tfrac{C}{Ro}\left(\tfrac{L}{\delta_M}\right)^3 |||\omega|||_{2,k+1}^2 \\
&+ (\alpha^{4N+4} + \alpha^2 h^{2k} + h^{2k+2}) \tfrac{C}{Ro}\left(\tfrac{L}{\delta_M}\right)^3 \left(\sum_{n=0}^{N+1} |||F^n \omega|||_{2,k+1}^2 \right) + h^{2k} C\left(\tfrac{L}{\delta_M}\right)^3 |||\nabla\omega|||_{4,1}^4 \\
&+ h^{2k} C\left(\tfrac{L}{\delta_M}\right)^3 |||\psi|||_{4,k+1}^4 + h^{2k+2} C\left(\tfrac{L}{\delta_M}\right)^3 |||\omega|||_{4,k+1}^4 \\
&+ (\alpha^{4N+4} + \alpha^2 h^{2k} + h^{2k+2}) C\left(\tfrac{L}{\delta_M}\right)^3 \left(|||\nabla\omega|||_{4,1}^4 + \sum_{n=0}^{N+1} |||F^n\omega|||_{4,k+1}^4 \right) \\
&+ h^{2k+2}\left(\tfrac{L}{\delta_M}\right)^3 C |||\psi|||_{4,k+1}^4 + (\alpha^{4N+4} + \alpha^2 h^{2k} + Ch^{2k+2})\left(\tfrac{L}{\delta_M}\right)^3 C |||\omega|||_{4,k+1}^4 \\
&+ (\alpha^{4N+4} + \alpha^2 h^{2k} + h^{2k+2}) C\left(\tfrac{L}{\delta_M}\right)^3 \sum_{n=0}^{N+1} |||F^n\omega|||_{4,k+1}^4 + \Delta t^4 \left(\tfrac{L}{\delta_M}\right)^3 \|\omega_{ttt}\|_{2,0}^2 \\
&+ \Delta t^4 \tfrac{C}{Ro}\left(\tfrac{\delta_M}{L}\right)^3 \|\nabla\omega_{tt}\|_{2,0}^2 + \Delta t^4 C\left(\tfrac{L}{\delta_M}\right)^3 \|\psi_{tt}\|_{2,0}^2 + \Delta t^4 C\left(\tfrac{L}{\delta_M}\right)^3 \left\| \left| \nabla \psi^{1/2} \right| \right\|_{4,1}^4 \\
&+ \Delta t^4 C\left(\tfrac{L}{\delta_M}\right)^3 \|\omega_{tt}\|_{4,1}^4 + \Delta t^4 \tfrac{C}{Ro}\left(\tfrac{L}{\delta_M}\right)^3 |||\nabla\omega|||_{4,1}^4 + \Delta t^4 C\left(\tfrac{L}{\delta_M}\right)^3 \|\psi_{tt}\|_{4,1}^4 \\
&+ \sum_{n=0}^{M-1} \Delta t \left(\tfrac{L}{\delta_M}\right)^3 \left(C + C\|\nabla\omega^{n+\frac{1}{2}}\|_1^2 + C\|\omega^{n+\frac{1}{2}}\|_{k+1}^2 \right) \|e_h^{n+\frac{1}{2}}\|^2.
\end{aligned}
$$

Considering $\Delta t < \dfrac{\left(\delta_M/L\right)^3}{C + C\|\nabla\omega^{n+\frac{1}{2}}\|_1^2 + C\|\omega^{n+\frac{1}{2}}\|_{k+1}^2}$ (such that we can apply Gronwall inequality) we have

$$
\begin{aligned}
&\|e_h^M\|^2 - \|e_h^0\|^2 + \tfrac{\Delta t}{Ro}\left(\tfrac{\delta_M}{L}\right)^3 \sum_{n=0}^{M-1} \|\nabla e_h^{n+\frac{1}{2}}\|^2 \le C^* \Big\{ h^{2k}\tfrac{C}{Ro}\Big(\tfrac{\delta_M}{L}\Big)^3 |||\omega|||_{2,k+1}^2 \\
&+ h^{2k}\tfrac{C}{Ro}\left(\tfrac{L}{\delta_M}\right)^3 |||\psi|||_{2,k+1}^2 + h^{2k+2}\tfrac{C}{Ro}\left(\tfrac{L}{\delta_M}\right)^3 |||\omega|||_{2,k+1}^2 \\
&+ (\alpha^{4N+4} + \alpha^2 h^{2k} + h^{2k+2})\tfrac{C}{Ro}\left(\tfrac{L}{\delta_M}\right)^3 \left(\sum_{n=0}^{N+1} |||F^n\omega|||_{2,k+1}^2\right) + h^{2k}C\Big(\tfrac{L}{\delta_M}\Big)^3 |||\nabla\omega|||_{4,1}^4 \\
&+ h^{2k}C\Big(\tfrac{L}{\delta_M}\Big)^3 |||\psi|||_{4,k+1}^4 + h^{2k+2}C\left(\tfrac{L}{\delta_M}\right)^3 |||\omega|||_{4,k+1}^4 \\
&+ (\alpha^{4N+4} + \alpha^2 h^{2k} + h^{2k+2})C\left(\tfrac{L}{\delta_M}\right)^3 \left(|||\nabla\omega|||_{4,1}^4 + \sum_{n=0}^{N+1} |||F^n\omega|||_{4,k+1}^4\right) \\
&+ h^{2k+2}\left(\tfrac{L}{\delta_M}\right)^3 C|||\psi|||_{4,k+1}^4 + (\alpha^{4N+4} + \alpha^2 h^{2k} + Ch^{2k+2})\left(\tfrac{L}{\delta_M}\right)^3 C|||\omega|||_{4,k+1}^4 \\
&+ (\alpha^{4N+4} + \alpha^2 h^{2k} + h^{2k+2})C\left(\tfrac{L}{\delta_M}\right)^3 \sum_{n=0}^{N+1} |||F^n\omega|||_{4,k+1}^4 + \Delta t^4\left(\tfrac{L}{\delta_M}\right)^3 \|\omega_{ttt}\|_{2,0}^2 \\
&+ \Delta t^4\tfrac{C}{Ro}\left(\tfrac{\delta_M}{L}\right)^3 \|\nabla\omega_{tt}\|_{2,0}^2 + \Delta t^4 C\Big(\tfrac{L}{\delta_M}\Big)^3 \|\psi_{tt}\|_{2,0}^2 + \Delta t^4 C\Big(\tfrac{L}{\delta_M}\Big)^3 \Big|\Big|\Big|\nabla\psi^{1/2}\Big|\Big|\Big|_{4,1}^4 \\
&+ \Delta t^4 C\Big(\tfrac{L}{\delta_M}\Big)^3 \|\omega_{tt}\|_{4,1}^4 + \Delta t^4\tfrac{C}{Ro}\Big(\tfrac{L}{\delta_M}\Big)^3 |||\nabla\omega|||_{4,1}^4 + \Delta t^4 C\left(\tfrac{L}{\delta_M}\right)^3 \|\psi_{tt}\|_{4,1}^4 \Big\}. \qquad (66)
\end{aligned}
$$

where

$$
C^* := \exp\left\{ \Delta t \sum_{n=0}^{M-1} \frac{\left(\frac{L}{\delta_M}\right)^3 \Big(C + C\|\nabla\omega^{n+\frac{1}{2}}\|_1^2 + C\|\omega^{n+\frac{1}{2}}\|_{k+1}^2\Big)}{1 - \Delta t\Big(\frac{L}{\delta_M}\Big)^3 \Big(C + C\|\nabla\omega^{n+\frac{1}{2}}\|_1^2 + C\|\omega^{n+\frac{1}{2}}\|_{k+1}^2\Big)} \right\}. \qquad (67)
$$

Thus we obtain (48) from the triangle inequality and (66).
For estimate (49), we apply (66) in

$$
\begin{aligned}
\left\|\nabla\left(\omega\left(t^{n+\frac{1}{2}}\right) - \omega_h^{n+\frac{1}{2}}\right)\right\|^2 &\le \left\|\nabla\left(\omega\left(t^{n+\frac{1}{2}}\right) - \omega^{n+\frac{1}{2}}\right)\right\|^2 + \left\|\nabla e_\perp^{n+\frac{1}{2}}\right\|^2 + \left\|\nabla e_h^{n+\frac{1}{2}}\right\|^2 \\
&\le \frac{\Delta t^3}{48}\int_{t^n}^{t^{n+1}} \|\omega_{tt}\|^2 dt + Ch^{2k}\left\|\omega^{n+\frac{1}{2}}\right\|_{k+1}^2 + \|\nabla e_h^{n+\frac{1}{2}}\|^2.
\end{aligned}
$$

□

Proof of Corollary 1. This follows directly from

$$
\|\nabla(\psi(t^{n+\frac{1}{2}}) - \psi_h^{n+\frac{1}{2}})\|^2 \le \|\nabla\left(\psi(t^{n+\frac{1}{2}}) - \psi^{n+\frac{1}{2}}\right)\|^2 + \|\nabla E^{n+\frac{1}{2}}\|^2, \qquad (68)
$$

after we apply inequality (59), Lemma 11, Lemma 1, sum from $n = 0, ..., M-1$ and apply Theorem 1. □

5. Numerical experiments

In this section, we provide two different experiments to present the results obtained with the proposed scheme. In the first we validate our computational implementation and estimate convergence rates using an analytical solution. In the second, we simulate the more realistic and traditional double-gyre wind forcing

benchmark. The software FreeFem++[7] was used to implement the proposed scheme. To solve the resulting nonlinear system, we used a Newtonian iteration at each timestep. In addition, a multi-frontal Gauss LU factorization implemented in the package UMFPACK (provided with FreeFem++ software) was used as our linear solver.

5.1. Convergence rates verification. Now we validate our computational implementation and confirm the convergence analysis presented above using a known analytical solution to estimate convergence rates. Considering the domain $\Omega = (0,1)\times(-1,1)$, $t \in (0,1]$, and for

$$\mathcal{F} = -\pi \exp\left[-\frac{2\pi^2}{Ro}\left(\frac{\delta_M}{L}\right)^3 t\right]\cos\pi x \sin\pi y,$$

the BV model has the following time dependent analytical solution (with homogeneous Dirichlet boundary conditions):

$$\psi = \exp\left[-\frac{2\pi^2}{Ro}\left(\frac{\delta_M}{L}\right)^3 t\right]\sin\pi x \sin\pi y,$$

$$\omega = 2\pi^2 \exp\left[-\frac{2\pi^2}{Ro}\left(\frac{\delta_M}{L}\right)^3 t\right]\sin\pi x \sin\pi y.$$

Using this known solution, convergence rates were estimated through simulations in quasi-uniform regular triangular meshes for $h = \frac{1}{4}$, $h = \frac{1}{8}$, $h = \frac{1}{16}$, $h = \frac{1}{32}$, $h = \frac{1}{64}$ and $h = \frac{1}{128}$, where h is the mesh-width. Figure 1 presents the coarsest mesh used in this experiment. In all cases we chose $\alpha = h$, and the timestep was chosen in terms of h in order to balance the error sources from the convergence theorem. That is, for P_1 elements and $\alpha = h$, the $L^2(0,T;H^1(\Omega))$ vorticity error and $L^\infty(0,T;H^1(\Omega))$ streamfunction error from the theorem are $O(\Delta t^2 + h)$, and thus we chose $\Delta t = \sqrt{h}$ (but slightly rounded so that Δt evenly divided T), and thus here we expect first order convergence in these norms as $\Delta t,\ h \to 0$. For P_2 and P_3 elements, we chose $\Delta t = h$ and $\Delta t = \sqrt{h^3}$, and expect second and third order convergence in these norms, respectively.

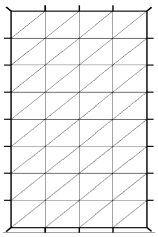

FIGURE 1. Mesh with $h = 1/4$ which corresponds to a grid with 4x8 squares.

Tables 1, 2 and 3 present the errors and convergence rates obtained for decreasing h and Δt, using $\frac{\delta_M}{L} = 0.02$ and $Ro = 1.0$. From these tables we observe that the convergence of the numerical solution to the exact solution is optimal and agrees with the convergence theory presented above, for any choices of elements. We remark that for $N = 0$, the $L^2(0,T;H^1(\Omega))$ error is $O(h^k + h^2)$, for $N = 1$ the

$L^2(0,T;H^1(\Omega))$ error is $O(h^k+h^4)$ and for $N=2$, the $L^2(0,T;H^1(\Omega))$ error is $O(h^k+h^6)$, which were confirmed through the rates estimated in the experiments. That is, provided a smooth solution, BV-α-$D1$ and BV-α-$D2$ will converge faster than the BV-α (D_0) being more accurate.

TABLE 1. Convergence rates for BV-α-D_0 ($N=0$) model with $\frac{\delta_M}{L}=0.02$ and $Ro=1.0$.

Element	h^{-1}	$\|w-w_h\|_{2,1}$	Rate	$\|w-w_h\|_{\infty,0}$	Rate	$\|\psi-\psi_h\|_{\infty,1}$	Rate
P_1	4	24.189		1.9868		2.1732	
($\Delta t=\sqrt{h}$)	8	12.376	0.97	0.61369	1.69	1.0117	1.10
	16	6.1545	1.01	0.16167	1.92	0.39299	1.36
	32	3.0614	1.01	0.041218	1.97	0.16706	1.23
	64	1.5259	1.00	0.010349	1.99	0.078803	1.08
	128	0.76181	1.00	0.002606	1.99	0.038768	1.02
P_2	4	6.3875		0.79216		1.7469	
($\Delta t=h$)	8	2.7885	1.20	0.28037	1.50	0.74236	1.23
	16	1.0076	1.47	0.078785	1.83	0.22523	1.72
	32	0.33616	1.58	0.020767	1.92	0.05949	1.92
	64	0.10476	1.68	0.0052803	1.98	0.015086	1.98
	128	0.02967	1.82	0.0013261	1.99	0.003785	1.99
P_3	4	7.5925		0.88577		1.7349	
($\Delta t=\sqrt{h^3}$)	8	3.6645	1.05	0.28925	1.61	0.7405	1.23
	16	1.1144	1.72	0.079633	1.86	0.22489	1.72
	32	0.36152	1.62	0.020844	1.93	0.059414	1.92
	64	0.10877	1.73	0.005286	1.98	0.015067	1.98

TABLE 2. Convergence rates for BV-α-D_1 ($N=1$) model with $\frac{\delta_M}{L}=0.02$ and $Ro=1.0$.

Element	h^{-1}	$\|w-w_h\|_{2,1}$	Rate	$\|w-w_h\|_{\infty,0}$	Rate	$\|\psi-\psi_h\|_{\infty,1}$	Rate
P_1	4	23.976		1.9716		1.6753	
($\Delta t=\sqrt{h}$)	8	12.202	0.97	0.54573	1.85	0.66267	1.34
	16	6.1025	1.00	0.14161	1.95	0.30999	1.10
	32	3.049	1.00	0.036064	1.97	0.15426	1.01
	64	1.5232	1.00	0.0090863	1.99	0.077105	1.00
	128	0.76126	1.00	0.0022755	2.00	0.038553	1.00
P_2	4	4.5291		0.36528		0.9807	
($\Delta t=h$)	8	1.1333	2.00	0.059717	2.61	0.18122	2.44
	16	0.27668	2.03	0.0061093	3.29	0.020044	3.18
	32	0.081142	1.77	0.00058915	3.37	0.0031885	2.65
	64	0.025527	1.67	8.0004e-5	2.88	7.497e-4	2.09
	128	0.0071309	1.84	9.5087e-6	3.07	1.8665e-4	2.01
P_3	4	4.4873		0.38391		0.95793	
($\Delta t=\sqrt{h^3}$)	8	0.86042	2.38	0.058728	2.71	0.17452	2.46
	16	0.077881	3.47	0.0055599	3.40	0.016097	3.44
	32	0.0068168	3.51	0.00039313	3.82	0.0011237	3.84
	64	0.00052529	3.70	2.5343e-5	3.96	7.2312e-5	3.96

TABLE 3. Convergence rates for BV-α-D_2 ($N = 2$) model with $\frac{\delta_M}{L} = 0.02$ and $Ro = 1.0$.

Element	h^{-1}	$\|w - w_h\|_{2,1}$	Rate	$\|w - w_h\|_{\infty,0}$	Rate	$\|\psi - \psi_h\|_{\infty,1}$	Rate
P_1	4	23.906	1.9666	1.4363			
($\Delta t = \sqrt{h}$)	8	12.184	0.97	0.5435	1.86	0.6239	1.20
	16	6.1012	1.00	0.14125	1.94	0.3086	1.02
	32	3.0489	1.00	0.03604	1.97	0.15422	1.00
	64	1.5232	1.00	0.0090846	1.99	0.077104	1.00
	128	0.76126	1.00	0.0022754	2.00	0.038553	1.00
P_2	4	4.5291		0.36528		0.9807	
($\Delta t = h$)	8	1.1333	2.00	0.059717	2.61	0.18122	2.44
	16	0.27668	2.03	0.0061093	3.29	0.020044	3.18
	32	0.081142	1.77	0.00058915	3.37	0.0031885	2.65
	64	0.025527	1.67	8.0004e-5	2.88	7.497e-4	2.09
	128	0.0071309	1.84	9.5087e-6	3.07	1.8665e-4	2.01
P_3	4	4.4873		0.38391		0.95793	
($\Delta t = \sqrt{h^3}$)	8	0.86042	2.38	0.058728	2.71	0.17452	2.46
	16	0.077881	3.47	0.0055599	3.40	0.016097	3.44
	32	0.0068168	3.51	0.00039313	3.82	0.0011237	3.84
	64	0.00052529	3.70	2.5343e-5	3.96	7.2312e-5	3.96

5.2. Double gyre wind experiment. As presented in [6, 8], when the BV equations are forced in a rectangular basin by a double gyre wind forcing on the ocean surface and dissipation is weak, despite the instantaneous streamfunction field being highly variable, time averaged streamfunction field is a well defined four gyre pattern. This pattern is composed by two inner gyres, which are driven by the wind, and two extremal gyres, at the northern and southern ends of the basin, which are driven by the eddy flux of potential vorticity. Moreover, according to [8], the extremal gyres are not a linear effect, but a result of a mean balance between the eddy flux of potential vorticity and wind forcing being susceptible to destruction by excessive dissipation.

The double gyre forcing experiment has been used as a model of more realistic ocean dynamics in several studies, and recently it has been used as a benchmark test to analyze new techniques to deal with turbulence in geophysical flows [16, 8, 22]. In the double gyre wind forcing experiment, the wind effect on the ocean's surface is prescribed setting $\mathcal{F} = \mathcal{F}_0 \sin(\pi y)$ with $\mathcal{F}_0 = 1$.

In this section we follow [22] and adopt the standard LES methodology: first we run a high resolution simulation with BV-model (no treatment of turbulence). Next, we run several experiments in a coarse resolution mesh with BV model and BV-α-Deconvolution model and compare them with the high resolution BV model solution as reference.

Following the experiments presented in [6, 16, 8, 22], we run simulations in different regular triangular meshes in the dimensionless rectangular domain $(0, 1) \times (-1, 1)$ using P_2 finite elements and consider meshes of different resolutions with $h = 1/4$ (which corresponds to a grid with 4x8 squares), $1/8$ (8x16), $1/16$ (16x32), $1/32$ (32x64) and $1/64$ (64x128) where h is the mesh-width. In the remainder of this section we will refer to our meshes as $n \times 2n$ for $n = 4, 8, 16, 32, 64$.

Experiments were made starting from $t = 0$ up until $t = 100$ as in [22] and we adopt $\Delta t = 0.001$ in all simulations. In this and in the next section we present figures of the average fields of streamfunction (ψ) and potential vorticity (given by $q = Ro\omega + y$), calculated using results from $t = 20$ until 100 as in [22]. For the double gyre wind forcing experiment we considered two interesting cases: i) ${}^{\delta_M}/_L = 0.02$ and $Ro = 0.0016$ (which is presented in [22]) and ii) ${}^{\delta_M}/_L = 0.01$ and $Ro = 0.0002$.

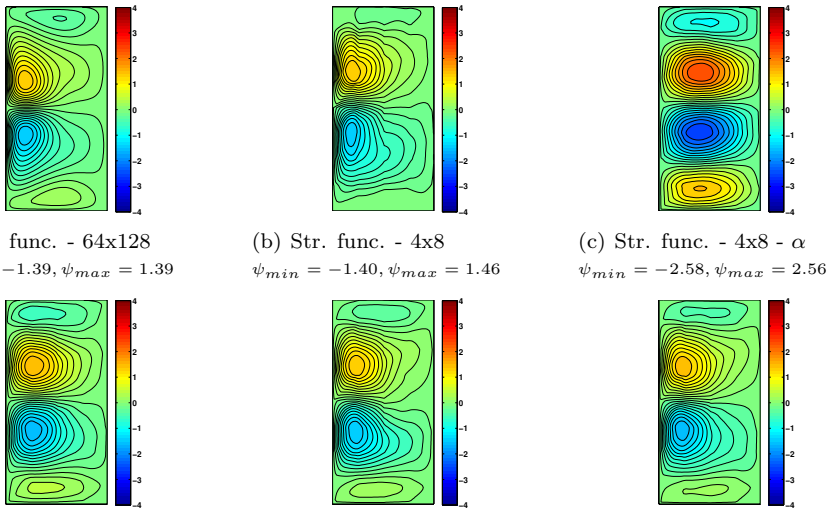

(a) Str. func. - 64x128
$\psi_{min} = -1.39, \psi_{max} = 1.39$

(b) Str. func. - 4x8
$\psi_{min} = -1.40, \psi_{max} = 1.46$

(c) Str. func. - 4x8 - α
$\psi_{min} = -2.58, \psi_{max} = 2.56$

(d) Str. func. - 4x8 - D_1
$\psi_{min} = -1.59, \psi_{max} = 1.63$

(e) Str. func. - 4x8 - D_2
$\psi_{min} = -1.48, \psi_{max} = 1.43$

(f) Str. func. - 4x8 - D_3
$\psi_{min} = -1.60, \psi_{max} = 1.52$

FIGURE 2. Streamfunction fields in the experiment with ${}^{\delta_M}/_L = 0.02$ and $Ro = 0.0016$ for (a) the high resolution BV model solution, (b) coarse (4×8) BV model solution and coarse (4×8) (c) BV-α, (d) BV-α-D_1, (e) BV-α-D_2 and (f) BV-α-D_3.

5.2.1. Experiment for $Ro = 0.0016$. First, we present our results for the double gyre experiment considering the same case as in [22], that is, $Ro = 0.0016$ and $\left(\frac{\delta_M}{L}\right)^3 = 0.02$. In Figures 2(a) and 3(a) we present respectively the streamfunction and vorticity solutions obtained in the high resolution (64×128 mesh) experiment with the BV model. In these figures we can see that the streamfunction and vorticity solutions obtained in this experiment are very similar with the results presented in [22] in their DNS experiment.

As reported in [22, 8], decreasing the mesh resolution, the streamfunction solution obtained with the BV model degenerates in two gyres as it can be seen in Figure 2(b). In this case, using the BV-α model ($\alpha = \frac{1}{12}$) we can recover the four gyre pattern (Figure 2(c)), but the streamfunction is intensified in comparison with the streamfunction solution obtained in the high resolution experiment (Figure 2(a)) and the vorticity field is very noisy (Figure 3(c)). However, when we increase the order in the deconvolution operator (Figures 2(d), 2(e) and 2(f)), we can obtain more accurate solutions in comparison with the BV and BV-α model. In

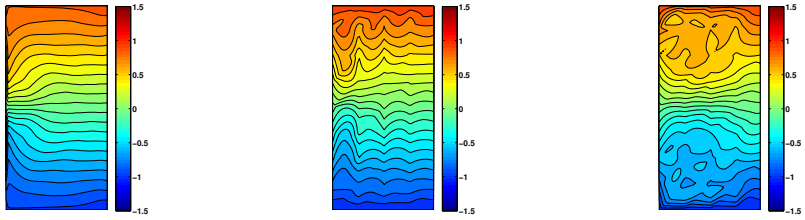

(a) Vort. - 64x128 (b) Vort. - 4x8 (c) Vort. - 4x8 - α

(d) Vort. - 4x8 - D_1 (e) Vort. - 4x8 - D_2 (f) Vort. - 4x8 - D_3

FIGURE 3. Vorticity fields in the experiment with $\delta_M/L = 0.02$ and $Ro = 0.0016$ for (a) the high resolution BV model solution, (b) coarse (4×8) BV model solution and coarse (4×8) (c) BV-α, (d) BV-α-D_1, (e) BV-α-D_2 and (f) BV-α-D_3.

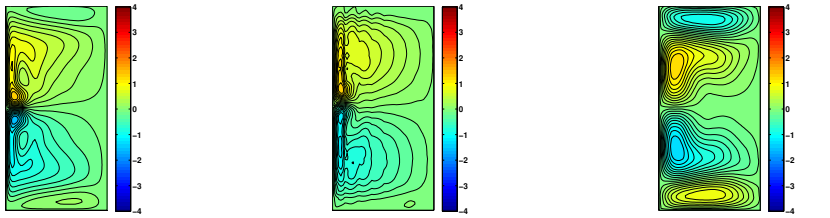

(a) Str. func. - 32x64
$\psi_{min} = -1.53, \psi_{max} = 1.49$

(b) Str. func. - 8x16
$\psi_{min} = -1.22, \psi_{max} = 1.41$

(c) Str. func.- 8x16 - α
$\psi_{min} = -1.34, \psi_{max} = 1.34$

(d) Str. func.- 8x16 - D_1
$\psi_{min} = -1.25, \psi_{max} = 1.30$

(e) Str. func.- 8x16 - D_2
$\psi_{min} = -1.31, \psi_{max} = 1.42$

(f) Str. func.- 8x16 - D_3
$\psi_{min} = -1.37, \psi_{max} = 1.37$

FIGURE 4. Streamfunction fields in the experiment with $\delta_M/L = 0.01$ and $Ro = 0.0002$ for (a) the high resolution BV model solution, (b) coarse (4×8) BV model solution and coarse (4×8) (c) BV-α, (d) BV-α-D_1, (e) BV-α-D_2 and (f) BV-α-D_3.

this figures, clearly we can see that the larger is the deconvolution order, the more accurate is the BV-α-deconvolution solution. In the BV-α-deconvolution vorticity solution we observe the same pattern (Figure 2(d), 2(e) and 2(f)). This improvement is related to the consistency error present in the BV-α-deconvolution model that, according to our convergence analysis, has order $2N + 2$, which for larger values of N permits more accuracy in the solution.

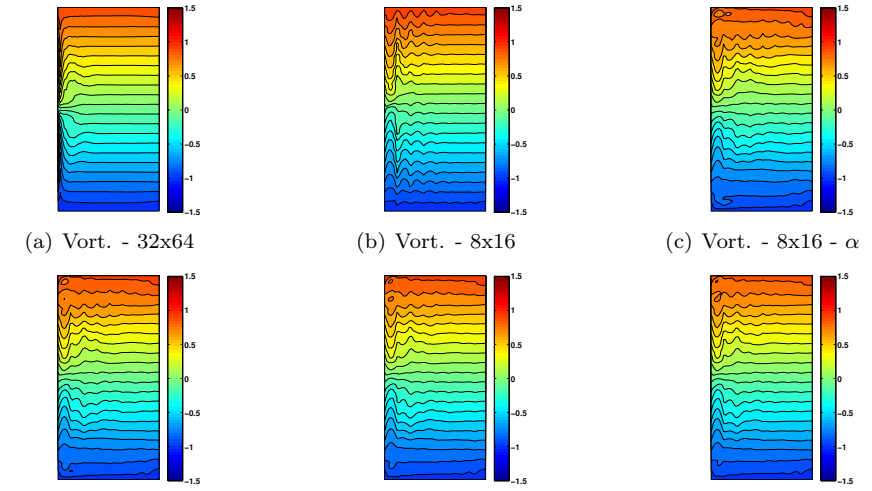

(a) Vort. - 32x64 (b) Vort. - 8x16 (c) Vort. - 8x16 - α

(d) Vort. - 8x16 - D_1 (e) Vort. - 8x16 - D_2 (f) Vort. - 8x16 - D_3

FIGURE 5. Vorticity fields in the experiment with $^{\delta_M}/_L = 0.01$ and $Ro = 0.0002$ for (a) the high resolution BV model solution, (b) coarse (8x16) BV model solution and coarse (8x16) (c) BV-α, (d) BV-α-D_1, (e) BV-α-D_2 and (f) BV-α-D_3.

5.2.2. Experiment for $Ro = 0.0002$. Now we present the results obtained for the double gyre experiment considering $Ro = 0.0002$ and $\left(\frac{\delta_M}{L}\right)^3 = 0.01$. Figures 4(a) and 5(a) present the streamfunction and vorticity solutions obtained in the high resolution mesh (32×64 mesh). We observe that in this experiment, the solution presents a distinct six gyre pattern. Futhermore, as we can see in Figure 4(b), this pattern is also susceptible to the mesh resolution. That is, when we simulate this experiment using the BV model in a coarse 8×16 mesh the six gyre pattern degenerates into two gyres. Moreover, the vorticity field produced in the coarse mesh becomes noisy.

Using the BV-α ($\alpha = \frac{1}{8}$) model we recover the four gyre pattern (Figure 4(c)), but not the six gyre pattern observed in the high resolution solution and, as for $Ro = 0.0016$, it is intensified compared to the high resolution solution. On the other hand, the streamfunction solutions produced with the BV-α-Deconvolution model for $N \geq 1$ are less intensified (Figures 4(d), 4(e) and 4(f)). Moreover, for $N = 3$ the BV-α-deconvolution model recovers the six gyre pattern (Figure 4(f)). In the vorticity field (Figures 5(d), 5(e) and 5(f)) we observed that, increasing the deconvolution order, the solution becomes less noisy and more similar to the high resolution solution.

Again, the results presented in this experiment corroborate the convergence analysis presented herein: increasing the deconvolution order makes solutions become more accurate.

6. Conclusion and final remarks

We have proposed and analysed an FEM scheme for the BV-α-Deconvolution model of geophysical flows that regularizes the flow and enables accuracy compared to the BV-α model. We proved that the scheme is both unconditionally stable and optimally convergent. Furthermore, we confirmed the predicted convergence rates through numerical simulations. Finally, we tested the BV-α-Deconvolution model in the traditional double gyre wind experiment, which is a more realistic model of the ocean dynamics, and found very good results. In this test we corroborate that increasing the deconvolution order in the model produces a more accurate solution.

In the present article we tested the BV-α-Deconvolution in a situation in which only the barotropic mode of ocean dynamics is present. As in [21], in a future work we intend to extend the BV-α-Deconvolution model for two layers in order apply this regularization to a more baroclinic situation. That will be an important step in the direction of true ocean dynamics.

References

[1] N. Adams and S. Stolz, Deconvolution methods for subgrid-scale approximation in large eddy simulation, Modern Simulation Strategies for Turbulent Flow, (2001) 21–41.
[2] S. C. Brenner and L. R. Scott, The Mathematical Theory of Finite Element Methods, vol. 15, Springer, 2008.
[3] D. Bresch and D. Gérard-Varet, Roughness-Induced Effects on the Quasi-Geostrophic Model, Communications in Mathematical Physics, 253 (2005) 81–119.
[4] G. Evensen, Sequential data assimilation with a nonlinear quasi-geostrophic model using monte carlo methods to forecast error statistics, Journal of Geophysical Research: Oceans, 99 (1994) 10143–10162.
[5] H. Goosse, H. Renssen, A. Timmermann and R. S. Bradley, Internal and forced climate variability during the last millennium: A model-data comparison using ensemble simulations, Quaternary Science Reviews, 24 (2005) 1345–1360.
[6] R. J. Greatbatch and B. Nadiga, Four-gyre circulation in a barotropic model with double-gyre wind forcing, Journal of Physical Oceanography, 30 (2000) 1461–1471.
[7] F. Hecht, New development in FreeFem++, Journal of Numerical Mathematics, 20 (2012) 251–265.
[8] D. D. Holm and B. T. Nadiga, Modeling Mesoscale Turbulence in the Barotropic Double-Gyre Circulation, Journal of Physical Oceanography, 33 (2003) 2355–2365.
[9] A. Katavouta and K. Thompson, Downscaling ocean conditions: Experiments with a quasi-geostrophic model, Ocean Modelling, 72 (2013) 231–241.
[10] B. Khouider and E. Titi, An Inviscid Regularization for the Surface Quasi-Geostrophic Equation, Communications on Pure and Applied Mathematics, 61 (2008) 1331–1346.
[11] W. Layton, An Introduction to the Numerical Analysis of Viscous Incompressible Flows, SIAM, Philadelphia, 2008.
[12] W. Layton, C. C. Manica, M. Neda and L. G. Rebholz, Numerical analysis and computational testing of a high accuracy Leray-deconvolution model of turbulence, Numerical Methods for Partial Differential Equations, 24 (2008) 555–582.
[13] W. Layton, C. C. Manica, M. Neda and L. G. Rebholz, Numerical analysis and computational comparisons of the NS-alpha and NS-omega regularizations, Computer Methods in Applied Mechanics and Engineering, 199 (2010) 916–931.
[14] A. J. Majda, C. Franzke and D. Crommelin, Normal forms for reduced stochastic climate models, Proceedings of the National Academy of Sciences, 106 (2009) 3649–3653.

[15] C. C. Manica, M. Neda, M. Olshanskii and L. G. Rebholz, Enabling numerical accuracy of Navier-Stokes-α through deconvolution and enhanced stability, ESAIM: Mathematical Modelling and Numerical Analysis, 45 (2011) 277–307.
[16] B. T. Nadiga and L. G. Margolin, Dispersive-dissipative eddy parameterization in a barotropic model, Journal of Physical Oceanography, 31 (2001) 2525–2531.
[17] B. T. Nadiga and S. Shkoller, Enhancement of the inverse-cascade of energy in the two-dimensional Lagrangian averaged Navier-Stokes equations, Physics of Fluids, 13 (2001) 1528–1531.
[18] L. G. Rebholz, A family of new, high order NS-α models arising from helicity correction in Leray turbulence models, Journal of Mathematical Analysis and Applications, 342 (2008) 246–254.
[19] H. Renssen, V. Brovkin, T. Fichefet and H. Goosse, Simulation of the Holocene climate evolution in Northern Africa: the termination of the African Humid Period, Quaternary International, 150 (2006) 95–102.
[20] G. Rivire, P. Arbogast and A. Joly, Eddy kinetic energy redistribution within idealized extratropical cyclones using a two-layer quasi-geostrophic model, Quarterly Journal of the Royal Meteorological Society, (2014) 1–18.
[21] O. San, A. Staples and T. Iliescu, Approximate deconvolution large eddy simulation of a stratified two-layer quasigeostrophic ocean model, Ocean Modeling, 63 (2013) 1 – 20.
[22] O. San, A. Staples, Z. Wang and T. Iliescu, Approximate deconvolution large eddy simulation of a barotropic ocean circulation model, Ocean Modeling, 40 (2011) 120 – 132.
[23] S. Stolz, N. Adams and L. Kleiser, An approximate deconvolution model for large-eddy simulation with application to incompressible wall-bounded flows, Physics of Fluids, 13 (2001) 997–1015.
[24] S. Stolz and N. A. Adams, An approximate deconvolution procedure for large-eddy simulation, Physics of Fluids, 11 (1999) 1699–1701.
[25] G. Sutyrin and X. Carton, Vortex interaction with a zonal Rossby wave in a Quasi-Geostrophic model, Dynamics of Atmospheres and Oceans, 41 (2006) 85–102.
[26] V. Thomée, Galerkin Finite Element Methods for Parabolic Problems, Springer, Berlin, second ed., 2010.
[27] S.-C. Yang, M. Corazza, A. Carrassi, E. Kalnay and T. Miyoshi, Comparison of ensemble-based and variational-based data assimilation schemes in a Quasi-Geostrophic model, in AMS 10th Symposium on Integrated Observing and Assimilation Systems for the Atmosphere, Oceans, and Land Surface, 2007.

Programa de Pós Graduação em Matemática Aplicada, Universidade Federal do Rio Grande do Sul and Instituto Federal do Rio Grande do Sul - Campus Rio Grande
E-mail: igoromonteiro@gmail.com.br

Instituto de Matemática Pura e Aplicada, Universidade Federal do Rio Grande do Sul
E-mail: carolina.manica@ufrgs.br